Review Article

Design and synthesis of magnetic nanoparticles for biomedical diagnostics

Yuan Chen[1,2], Xianguang Ding[2], Yan Zhang[1,2], Auginia Natalia[2], Xuecheng Sun[2], Zhigang Wang[2], Huilin Shao[1,2,3,4]

[1]Department of Biomedical Engineering, Faculty of Engineering, [2]Biomedical Institute for Global Health Research and Technology, National University of Singapore, Singapore 117599, Singapore; [3]Institute of Molecular and Cell Biology, Agency for Science, Technology and Research, Singapore 138673, Singapore; [4]Department of Surgery, Yong Loo Lin School of Medicine, National University of Singapore, Singapore 117599, Singapore

Correspondence to: Huilin Shao, PhD. National University of Singapore, MD6, 14 Medical Drive, #14-01, Singapore 117599, Singapore. Email: huilin.shao@nus.edu.sg.

Abstract: Sensitive and quantitative characterization of clinically relevant biomarkers can facilitate disease diagnosis and treatment evaluation. Magnetic nanomaterials and their biosensing strategies have recently received considerable attention. Magnetic signals experience little interference from native biological background as most biological molecules have negligible magnetic susceptibilities and thus appear transparent to external magnetic fields. Because of this unique property, magnetic sensing can be applied to both *in vivo* deep tissue imaging as well as *ex vivo* point-of-care diagnostics. To exploit this mode of magnetic detection, new advancements in both magnetic material syntheses and sensing technologies have been made. This review focuses on recent developments of magnetic nanomaterials as image contrast agents and diagnostic sensors. These developments have not only enabled precise control of magnetic nanomaterial properties but also expanded the reach of magnetic detection for biomedical diagnostics.

Keywords: Magnetic nanoparticles (NPs); *in vivo* imaging; *ex vivo* detection; miniaturized sensors

Submitted Oct 08, 2018. Accepted for publication Oct 17, 2018.
doi: 10.21037/qims.2018.10.07
View this article at: http://dx.doi.org/10.21037/qims.2018.10.07

Introduction

Early disease detection is highly desirable to improve health outcomes and reduce social-economic burdens (1-3). Specifically, rapid and sensitive characterization of disease biomarkers will not only be of immediate value for diagnostic screening, but also facilitates monitoring of disease progression and treatment efficacy (4,5). Recently, diagnostic strategies based on magnetic nanoparticles (NPs) have received considerable attention (6-9). These magnetic approaches experience little interference from native biological samples, as biological specimens typically have negligible magnetic susceptibilities, making them transparent to the external magnetic field even in the absence of extensive sample preparation. Central to these diagnostic approaches, new generations of magnetic nanomaterials have been specifically designed and developed for biomedical applications (10-13). These diverse magnetic nanomaterials not only possess high biocompatibility, but also support efficient image contrast and enable versatile surface modifications. Importantly, based on their unique applications in different detection modalities—as *in vivo* probes of magnetic imaging or *ex vivo* labels of biosensing assays—new nanomaterials could be specifically designed to fulfill new diagnostic needs (*Figure 1*).

Over the years, various magnetic detection technologies have been developed. As one of the most powerful diagnostic technologies among various imaging tools, magnetic resonance imaging (MRI) can provide pathophysiological information, through the generation of anatomical and

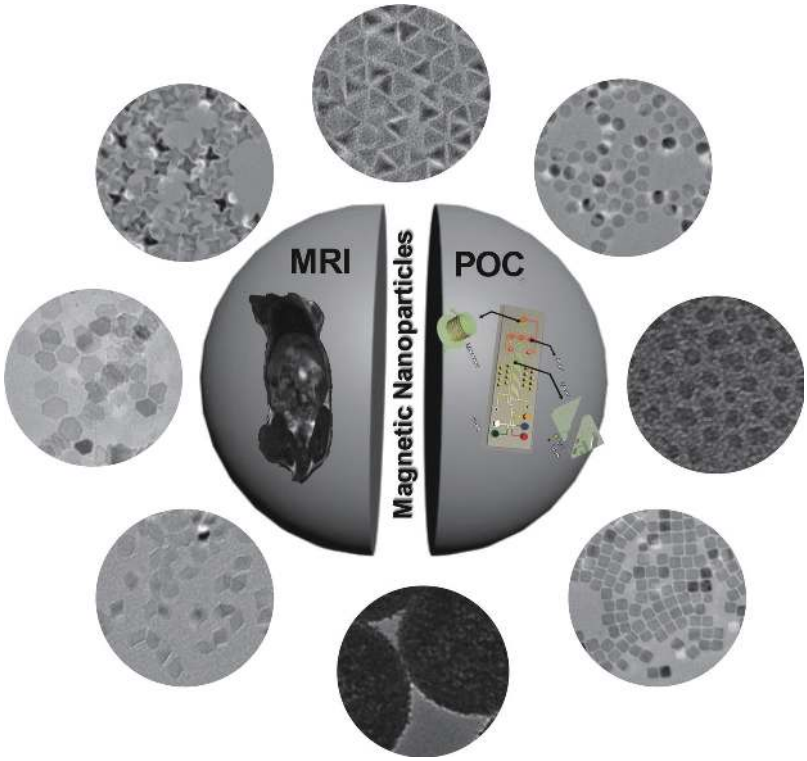

Figure 1 Illustration of various magnetic nanomaterials for biomedical diagnostics. Magnetic nanomaterials can be used as *in vivo* probes for magnetic resonance imaging (MRI) or *ex vivo* labels for point-of-care (POC) diagnostics. With the advancements in synthesis approach and sensing technologies, nanomaterials can be specifically designed and developed to fulfill new diagnostic needs.

functional images at a high spatial resolution. To further improve the imaging sensitivity as well as to analyze specific anatomical sites of interest, various inorganic magnetic nanomaterials have been developed and employed as MRI contrast agents (14,15). These materials possess not only exceptional potency in accelerating the spin relaxation time of water protons (image contrast), but also excellent colloidal stability, biocompatibility, and long circulation time for *in vivo* applications (16-19). More recently, with the advancement of MRI technologies, responsive agents which can react to local biological environments have been developed to provide functional and molecular information (20-22).

Beyond *in vivo* imaging, magnetic nanomaterials have also been applied to establish new generations of diagnostic assays for *ex vivo* detection. To quantify biologically relevant signals through magnetic nanomaterials, various detection technologies have been developed. These include techniques that use nuclear magnetic resonance (NMR) detectors to measure changes in the relaxation rate of surrounding water molecules, akin to the detection mechanism of MRI (7,9), as well as the applications of magnetometers [e.g., magneto-resistive sensors (23,24), Hall sensors (25,26)] to quantify magnetic fields directly from labeled biological targets. Through specific integration of nanomaterials with miniaturized detection platforms, these magnetic diagnostic assays have shown promising potential to provide robust, sensitive platform for point-of-care diagnostic applications.

By developing optimized magnetic nanomaterials, the detection sensitivities and capabilities of MRI and other magnetic sensors have been significantly improved. To date, various magnetic biosensors have been designed to quantify a wide range of targets, including proteins (27,28), extracellular vesicles (29-31), bacteria (32,33), and mammalian cells (34,35). This review focuses on the design and preparation of magnetic NPs as well as their applications for *in vivo* imaging and point-of-care sensors.

Magnetic properties and material synthesis

The classification of a material's magnetic properties is based on its magnetic susceptibility (χ), which is defined by

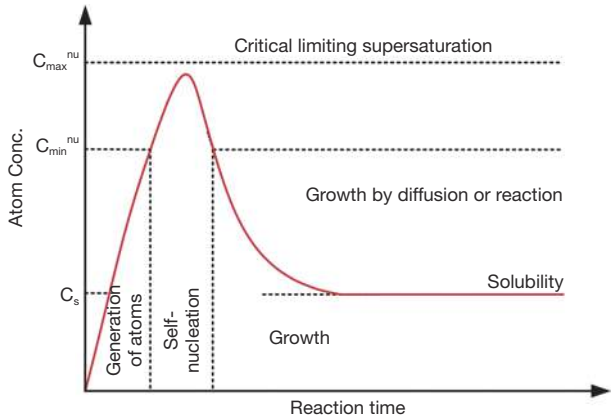

Figure 2 The LaMer model. Plot of the LaMer model for the generation of atoms, nucleation, and subsequent growth of colloidal synthesis. Reprinted with permission from (43). Copyright 1950 American Chemical Society.

the ratio of the induced magnetization (*M*) to the applied magnetic field (*H*). While in ferri- and ferromagnetic materials, magnetic moments align parallel to *H*. Coupling interactions between the electrons of the material result in ordered magnetic states. At small particle sizes (in the order of tens of nanometers), ferri- or ferromagnetic materials, such as magnetic NPs, become single magnetic domains and therefore maintain one large magnetic moment. However, at sufficiently high temperature, thermal energy can induce free rotation of the particles, resulting in a loss of net magnetization in the absence of an external field. This superparamagnetic property ensures that magnetic NPs do not spontaneously aggregate under physiological solutions (36).

By producing local magnetic dipoles with strong spatial dependence, magnetic NPs efficiently destroy the coherence in the spin-spin relaxation of water protons. The net effect is a change in magnetic resonance signal measured as (I) T_1 longitudinal relaxation, which results in longitudinal magnetization recovery, and (II) T_2 transverse relaxation, which involves transverse magnetization decay originating from the loss of phase coherence and dephasing between the proton nuclear spins. The capacities of magnetic NPs to decrease T_2 and T_1 are defined as their transverse (r_2) and longitudinal (r_1) relaxivities, respectively. As a result of these intrinsic properties, magnetic NPs can be used as contrast agents in MRI studies and as labeling and signal transducers in biosensing studies. Several factors could be considered in controlling the magnetic properties of these nanomaterials, including their material composition, size-dependent magnetism, shape and structure, as well as surface coating. Here, we briefly introduce several typical NPs, their synthesis methods as well as their magnetic properties.

Material synthesis

Magnetic NPs have been prepared in chemical precipitation process (37), hydrothermal process (38), ball milling (39), microemulsion (40), and Sol-Gel method (41,42). The formation mechanism of monodisperse NPs can be explained by the "LaMer model" which systematically describes NPs formation and growth during particle synthesis (43). Specifically, this model involves three different steps, namely nucleation, crystal growth, and Ostwald ripening (*Figure 2*). By optimizing the conditions at these steps, NPs with variable sizes, shapes, and components can be prepared in a controlled manner.

Magnetic metal NPs

Iron (Fe) is one of the most common ferromagnetic materials used for magnetic applications (44). To date, many methods have been used to synthesize Fe NPs. These methods include reduction of iron salts in aqueous solutions, in the presence of reducing agents such as sodium borohydride. In order to ensure particle uniformity, Fe NPs can also be synthesized by thermal decomposition of $Fe(CO)_5$ based on a polymer matrix (45). Additionally, by changing the precursors to $Fe[N(SiMe_3)_2]_2$, the overall synthesis yield can be improved and by-product formation is reduced (46).

In addition to Fe, cobalt (Co) is another commonly used material. In the synthesis of Co nanomaterials [as well as Ni and FeM (Co, Pt) composite materials], organic phase preparation has been widely adopted (47-49). In this synthesis approach, surfactants play a key role in controlling the particle size. Specifically, surfactants control the formation of droplets of varying sizes; these droplets define the templates in which nucleation and NPs growth will happen. For example, tributylphosphine (TBP) has been frequently used to control Co nucleation and growth, while oleic acid is used for particle stabilization (50). Alternatively, Co NPs can also be prepared by reducing cobalt(II) bis(2-ethylhexyl)sulfosuccinic acid [Co-$(AOT)_2$] with $NaBH_4$ (51) or directly synthesized by reducing $Co(CH_3COO)_2{\cdot}4H_2O$ under high temperature (52).

In addition to the traditional face-centered cubic (fcc) and hexagonal-close-packed (hcp) structures, Co NPs also have a special structure—ε-structure which is mainly formed by reducing $CoCl_2$ with hydride (53). There is a strong correlation between crystal structure and the magnetic properties of cobalt. By changing the state of the metastable ε-Co NPs, the corresponding soft magnetic properties can also be tuned.

Magnetic oxide NPs

Magnetic oxide NPs are attractive due to their strong magnetic properties and chemical stabilities. Among them, Fe_3O_4 has cubic-closest-packed inverse spinel structure and semi-metallic properties, showing great potential in magnetic separation and biomedical fields (54,55). One of the conventional methods to synthesize Fe_3O_4 NPs is using a simple solvothermal reduction system based on Fe complexes (56). However, this method cannot effectively control the surface energy and ensure uniform growth of magnetic iron oxide NPs. Therefore, organic phase methods have been explored to prepare NPs with uniform sizes. Researchers have also used different concentrations of precursor components and dopants to prepare different nanostructures (57). For example, Zeng *et al.* tuned surfactant/metal precursor ratios to obtain cubic and polyhedral structures of Fe_3O_4 (58). Different morphologies of magnetic NPs show different magnetic properties. For example, compared with the cubic structured ferrite, the room temperature coercivity (H_c) of hexagonal barium ferrite (BaFe) NPs became much higher (over 4k Oe) by appropriately adjusting the proportion of the components (59). In addition, antiferromagnetic NPs [such as FeO (60), NiO (61), and MnO NPs (62)] can also be prepared by this kind of thermal decomposition based on suitable metal precursors.

Multicomponent magnetic NPs

As compared to single-component NPs, multicomponent NPs do not only realize multifunctionalities but also provide novel functions that are not available in single-component materials or structures. In addition, it can achieve enhanced properties and overcome the natural constraints of single materials. The progress on the design and synthesis of multifunctional NPs has been summarized in several recent comprehensive review articles (63-65). Here, we highlight two main kinds of multifunctional NPs (core/shell and dumbbell-like NPs), including their structures and magnetic properties.

Core/shell NPs

Core/shell NPs are the most common type of multicomponent NPs and have been studied extensively. Core/shell structures were first realized in semiconductor NPs (66), expanded to prevent the oxidation of metal, especially Fe which has extremely high reactivity. Lee *et al.* recently prepared hybrid magnetic NPs (Fe/Fe_3O_4) with a large Fe core and a thin ferrite shell. Briefly, iron (0) pentacarbonyl [$Fe(CO)_5$] was thermally decomposed into Fe core. The mixture was then treated with oxygen, resulting in a thin protective ferrite shell while retaining a larger Fe core. This material showed enhanced sensitivity for the detection of bacterial cells with r_2 relaxivity of up to 260 $(s{\cdot}mM\ Fe)^{-1}$ (67). Moreover, the ferrite shell could be further engineered ($Fe@MFe_2O_4$, M = Fe, Mn, Co) (68) (*Figure 3*). The resultant particles showed high relaxivity and remained monodispersed with little particle aggregation. $Fe@MFe_2O_4$ could sensitively detect proteins and individual cancer cells in the picomolar range. Another interesting core-shell structure is core/shell Fe/Fe_xC NPs prepared through thermal decomposition of $Fe(CO)_5$ under argon or hydrogen (69). The magnetic properties of these nanostructures are shown to be improved as compared to Fe_3O_4 or core-shell Fe/Fe_3O_4 NPs even after oxidation.

Besides Fe metal core, $FePt@Fe_3O_4$ offers another important functional improvement. For example, in the previously synthesized FePt seed solution, $Fe(acac)_3$ could be thermally decomposed to form $FePt@Fe_3O_4$ NPs (70). It is noteworthy that the particles with 0.5 nm Fe_3O_4 shell have H_c of 5 kOe, while those with 3 nm shell have a H_c value of only 1.4 kOe, indicating the dependence of H_c over the thickness of the Fe_3O_4 shell. Furthermore, through the addition of the shell component onto the magnetic cores, the magnetic properties of these core/shell NPs can be effectively adjusted due to the energy conversion efficiency and the thermal energy changes at the core/shell interface. As a typical representative which took advantage of the plasmon resonance properties of noble metals in magnetic systems, $Au@Fe_3O_4$ NPs were explored. It exhibited both superparamagnetic of Fe_3O_4 NPs and plasmonic properties of gold (71), while the magnetic properties of Fe_3O_4 were affected by the interactions between Au and Fe_3O_4. In order to synthesize multicomponent NPs with specific size and morphology, seed-mediated growth methods are often used. For example,

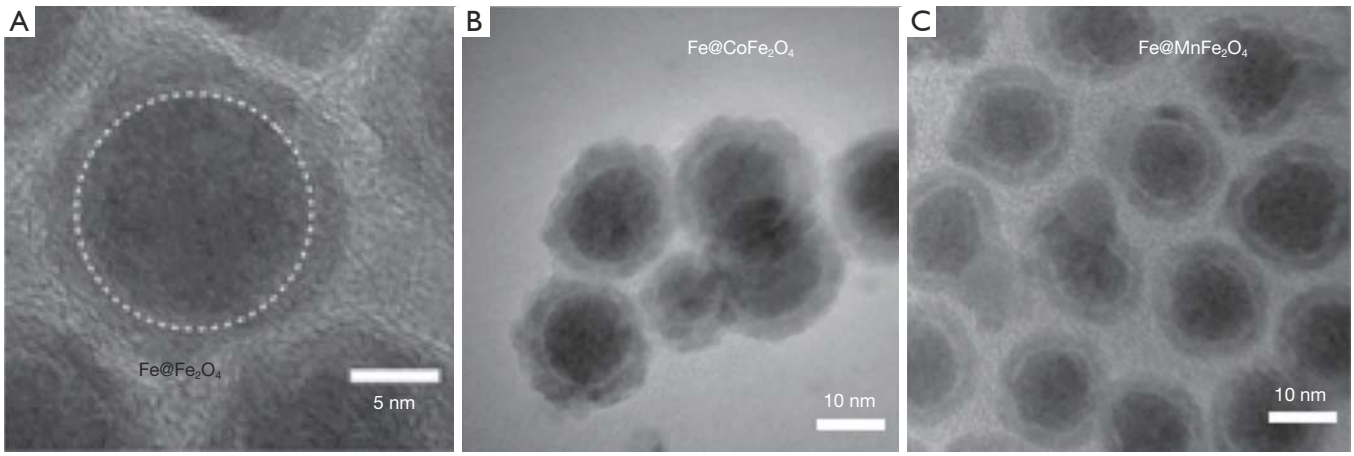

Figure 3 Core/shell magnetic nanomaterials. To prepare nanomaterials with strong relaxivity and good stability, Fe-core magnetic NPs with different shell compositions were prepared. Aside from Fe_2O_4 shell, the ferrite shell could be further engineered into $CoFe_2O_4$ and $MnFe_2O_4$. Reprinted with permission from (68). Copyright 2011 Wiley-VCH.

Ge *et al.* illustrated a strategy called "packaging and etching" (72). These core/shell NPs are particularly suitable as multifunctional probes for biomedical applications. In addition to regulating the composition of nanomaterials, particle morphology and structure can also be tuned to improve their magnetic properties. For example, Gao *et al.* selected FePt NPs as seeds to prepare FePt@CoS_2 egg yolk-shell nanocrystals by oxidation of FePt NPs (73).

Dumbbell NPs

Unlike the core/shell NPs which are typically formed by coating a uniform shell on the seed NPs, dumbbell NPs are usually formed by anisotropic nucleation and growth of one or even more discrete components on the surface of the seeds. The most studied dumbbell NPs are precious metal-magnetic oxide NPs (74). For instance, Au-Fe_3O_4 dumbbell NPs were obtained by the thermal decomposition of $Fe(CO)_5$ on the surface of prefabricated Au NPs followed by air oxidation (*Figure 4A,B,C*) (75). Similarly, $Fe(acac)_3$ and Fe-oleate were also used to synthesize Au-Fe_3O_4 dumbbell NPs via thermal decomposition reaction in high boiling point non-coordinating solvents (e.g., 1-octadecene) (71,77). Typically, during the growth process, the template material is gradually oxidized and the precious metal on the surface continuously grows. The anisotropic growth of dumbbell NPs is closely related to the polarity of the solvent and the surfactant; the polarity of the solvent or the surfactant could be regulated to control the size and morphology of the resultant NPs (78). By combining two different components, the physical and chemical properties of the dumbbell NPs can be significantly different from their single component counterparts. For example, the absorption peak of Au-Fe_3O_4 NPs is red-shifted from 520 to 538 nm owing to the light absorption of Fe_3O_4. Like the Fe_3O_4 NPs, the dumbbell particles are superparamagnetic at room temperature. The 3–14 nm dumbbell particles show loops similar to the 14 nm Fe_3O_4 NPs with saturation moment reaching 80 emu/g. The NPs are thus useful as dual optical/magnetic probe for diagnostic and therapeutic applications (75).

More complex dumbbell NPs can be synthesized using preformed two-component dumbbell NPs as seeds, for example Au_2-Au_1-Fe_3O_4 NPs (*Figure 4D,E*). The growth mechanism is related to the non-uniform strain-energy distribution caused by lattice distortion and failure criterion. In the Au_1-Fe_3O_4 solution, when Au_1 is small, the lattice distortion is large, and Au_2 prefers to grow as individual Au NPs. For the larger Au_1, the strain energy is located at the interface of Au_1-Fe_3O_4 NPs, and the lattice distortion at the far end of Au_1 is small. This favors the growth of Au_2 on Au_1 to form more complex structures (76). The author further identified that the interactions between Fe_3O_4 Au_1 and A_2 have important influences on the magnetic properties of Fe_3O_4.

Magnetic resonance imaging (MRI)

MRI measures the spin relaxation of water protons and is widely used in clinical imaging. As a non-invasive imaging

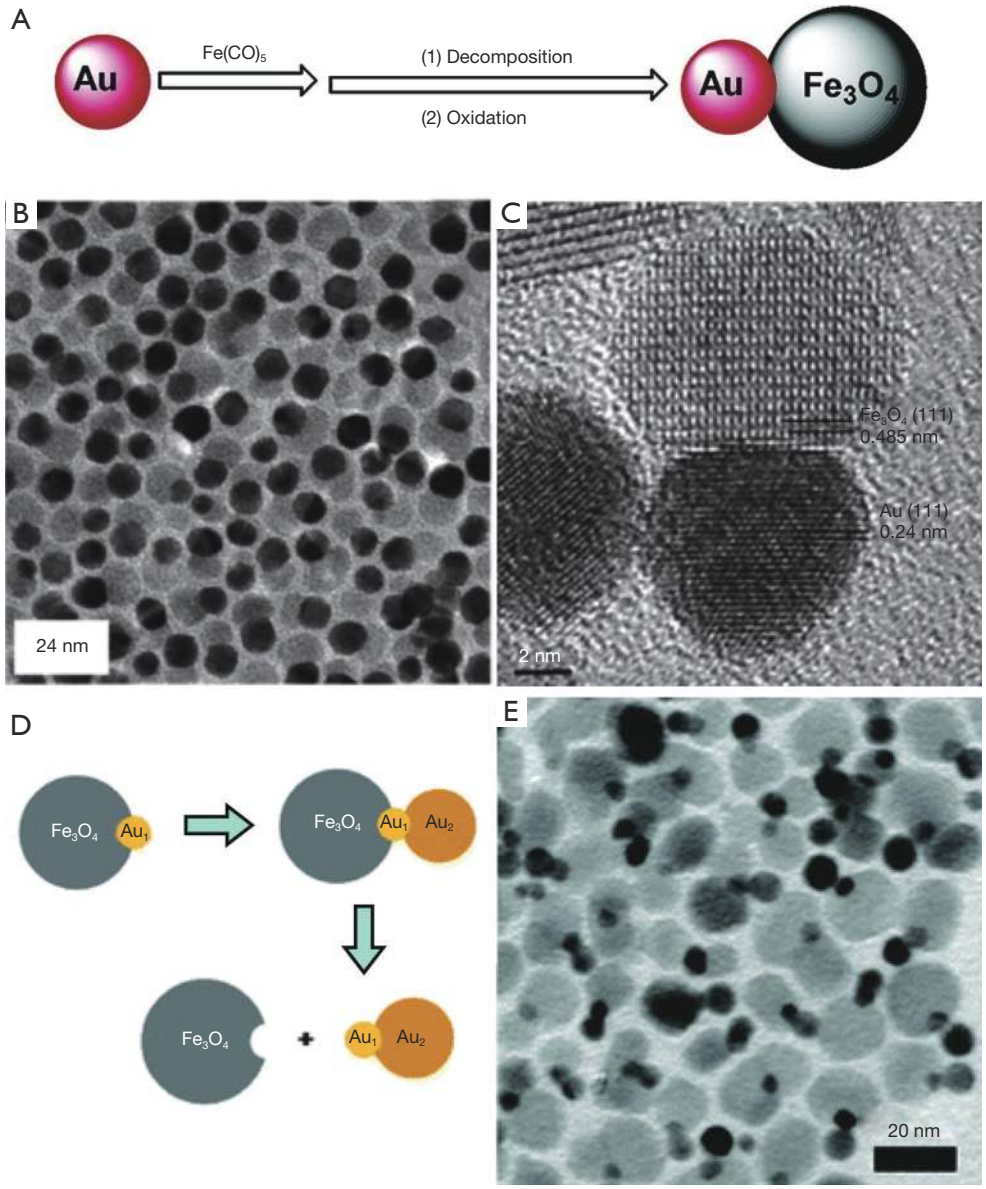

Figure 4 Dumbbell nanomaterials. (A) Schematic illustration of the synthesis of Au-Fe_3O_4 dumbbell NPs. (B) Representative transmission electron micrograph and (C) high-resolution image of the formed Au-Fe_3O_4 dumbbell NPs. (D) Schematic illustration of the Au_2 overgrowth on Au_1 NP and Au_1 NP detachment from the Fe_3O_4 NP, forming the new dumbbell-like Au_1-Au_2 and the dented Fe_3O_4 NP. (E) Transmission electron micrograph of the prepared Au_2-Au_1-Fe_3O_4 NPs. Reprinted with permission from (75). Copyright 2005 American Chemical Society. Reprinted with permission from (76). Copyright 2009 American Chemical Society.

tool, MRI enables a high spatial resolution at the cellular level (~10 μm) and deep tissue penetration without any ionizing irradiation, thereby offering good soft tissue contrast in normal and disease physiology. These distinct advantages make MRI one of the most powerful tools in clinical diagnostics, real-time treatment monitoring, and post-therapy evaluation. Furthermore, through the administration of exogenous contrast agents, which can accelerate the relaxation of water protons by causing local magnetic fields, the MRI sensitivity and signal-to-noise ratio can be greatly enhanced to favor accurate molecular imaging (15,79). Clinically, >30% of all MRI scans are performed with the

assistance of MRI agents. These contrast agents are either paramagnetic or superparamagnetic, with diameters ranging from a few nanometers to several hundred nanometers. They can be categorized into different groups according to their working mechanisms.

T_2 contrast agents

T_2 agents, which are also called negative contrast agents, are usually paramagnetic NPs in the form of various ion oxides (80). T_2 agents work by shortening T_2 of water protons, thereby generating negative (dark) images (81). Under the induction of external magnetic field, the T_2 agents can generate a local magnetic field which perturbs the spin-spin relaxation process of water protons nearby. As such, the contrast-enhancing capability of T_2 agents is highly related to their corresponding superparamagnetic properties and the applied external magnetic field.

As mentioned previously, the NPs' size and magnetic doping to form MFe_2O_4 (M = Co, Ni, Mn) have significant influence on the superparamagnetic properties. In addition, new studies have also shown that the particle morphology, as well as the inclusion of chelating agents can affect the T_2 image contrast capacity. For instance, Zhao and coworkers synthesized octapod iron oxide NPs and found that the material showed an ultrahigh transverse relaxivity (r_2) of 679.3±30 $mM^{-1}s^{-1}$, which was over 5 times higher than spherical iron oxide particles of similar geometric volumes (18). By preparing six different morphologies of manganese-doped iron oxide NPs, namely spheres, cubes, plates, tetrahedra, rhombohedra and octapod of the same volume, Yang *et al.* showed that the effective radii of the nanomaterials are crucial factors in affecting the T_2 relaxation rates of nearby protons (82). In addition, chelating agents have also been found to affect the transverse relaxation time by influencing the inhomogeneity of induced local magnetic field of magnetic NPs (83).

T_1 contrast agents

In comparison, T_1 agents or positive contrast agents are mainly paramagnetic NPs which work by shortening the longitudinal relaxation time (T_1) of water protons, thus producing positive (bright) images. While current clinical T_1 agents are primarily gadolinium (Gd) complexes, these agents have several disadvantages, including toxicity resulted from the leaching of Gd^{3+} from the complexes. In addition, the agents' relatively low *in vivo* circulation time further limits their clinical potential.

To overcome these disadvantages of Gd-based T_1 agents and develop new generations of magnetic T_1 agents for ultrasensitive imaging and early diagnosis, Mn and Fe-based T_1 MRI contrast agents have been extensively researched in recent years (19,21,84). In particular, the transition manganese metal ion (Mn^{2+}) is antiferromagnetic with five unpaired electrons and an essential element in human body. These features render the material a good T_1 candidate for *in vivo* usage. At present, a series of Mn-based NPs [e.g., MnO (85), Mn_3O_4 (86) and hollow MnO_2 NPs (87)] has been successfully developed for T_1 contrast imaging.

With five unpaired electrons, Fe-based NPs also show potential as T_1 contrast agents. A critical parameter in determining if the contrast agents can be considered as T_1 or T_2 agents is their ratio of relaxivity (i.e., r_2/r_1). An ideal T_1 contrast agent should exhibit high r_1/r_2 ratio to maximize their T_1 contrast effect, while suppress the influence of T_2 contrast. Generally, iron oxide NPs with a diameter >5 nm are not good for T_1 imaging due to their high r_2 value (i.e., large r_2/r_1 ratio). Specifically, recent studies have suggested that iron oxide NPs <5 nm can be highly desirable T_1 imaging (88). To enhance the material's T_1 contrast efficiency, iron oxide NPs could be modeled as core/shell structures. This type of material typically consists of a magnetic core to contribute to its T_2 performance as well as a magnetically disordered shell for improving its T_1 contrast. By decreasing the particle size, the magnetic core can be greatly reduced and thereby dramatically suppressing its magnetic moment. This reduction in particle size further improves the surface effect, which increases the dangling bonds of Fe^{3+} and the spin canting effect. These effects act in synergy to increase the particles' r_1 relaxivity while reducing their r_2 relaxivity.

Responsive MRI agents

Responsive MRI agents are activatable magnetic agents which are not only able to enhance the signal-to-noise imaging ratio at the sites of interest, but also produce simultaneous readouts of specific anatomical and physiological conditions (20,46,89-91). Specifically, new generations of responsive MRI agents can detect a wide range of stimuli, including hypoxia, redox states, enzymes, nucleic acids, metabolites, or changes in redox states and pH. As T_1 and T_2 relaxation times are mainly affected by two physiochemical factors of MRI contrast agents, namely water accessibility and superparamagnetism, new

research has been focusing on developing activatable MRI agents through changing their hierarchical organization (e.g., assembly or disassembly of NPs to influence the degree of water accessibility or the magnitude of the superparamagnetism) (92,93). For example, Chen and co-workers have recently designed a T_1-MRI contrast agent based on Mn^{2+} ions for efficient imaging of acidic tumor microenvironment (21). The prepared MnO_x encased in hollow mesoporous silica can be dissolved under weak acidic environment to release Mn^{2+} ions. This release significantly increases the relaxation rate r_1 of probes, achieving a 11-fold signal as compared to measurements with the neutral condition.

As previously described, the T_2 performance of MRI agents is tightly related to their superparamagnetic property, which is positively correlated to the size of the magnetic nanomaterials. Levering on this design principle, Wang *et al.* recently developed ultra small iron oxide NPs with the size of 3.5 nm (94). In acidic tumor environment, these NPs can assemble into clusters and hence improve the T_2 signal. Aside from this T_1 to T_2 contrast switching to sense the local pH, the magnetic clustering also facilitates the retention of the nanomaterials in the tumor, thereby improving the functional performance of the imaging system. In addition to pH, enzymatic activity can also be a triggering factor to cause (dis)aggregation of magnetic NPs. Recently, Gao *et al.* established a glutathione (GSH)-responsive MRI agent, which could enhance image contrast through cross-linking of adjacent Fe_3O_4 NPs (22). In the presence of GSH within the tumor microenvironment, the particles aggregated through *in situ* reaction between thiol groups and melamine moieties on the NPs. The aggregated particles showed a higher saturation magnetization and thus substantially improved the T_2 contrast.

Point-of-care detection

Due to their high sensitivity, compact instrumentation, and flexible integration, magnetic biosensors have emerged as excellent detection devices for point-of-care diagnostics. In recent years, a number of sensitive magnetic detection devices have been developed such as, magnetoresistive sensors (95), spin-valves (96), anisotropic magneto resistive-based sensors (97), superconducting quantum interference devices (SQUIDs) (98), Hall sensors (99), giant magneto-impedance based sensors (100), and micro-NMR sensors (101). In this section, we will use two sensing mechanisms, namely giant magnetoresistance (GMR) and NMR, to illustrate magnetic detection.

GMR sensor

The GMR effect is a change in electrical conductivity in a system that comprises multiple metallic layers. Under the influence of an external magnetic field, the magnetization of the ferromagnetic layers changes relative to one another, thereby changing the overall electrical conductivity of the system. In terms of sensor functionality and fabrication, GMR sensors possess many advantages, such as high sensitivity, low power, easy fabrication, and good compatibility with standard silicon-based integrated circuit technology. Hence, these sensors have demonstrated promising potential as sensing elements for biomarker detection (102). Specifically, recent studies have employed GMR sensors, in combination with magnetic beads as molecular labels, for diverse biomedical sensing applications (100,103-105). In these applications, GMR sensors were used to quantify magnetic fields directly from the labeled biological targets.

NMR sensor

NMR is another powerful magnetic phenomenon. Unlike the direct detection of magnetic moments by GMR sensors, NMR sensors detect via changes in the spin relaxation induced by magnetic fields (34,106). Aside from its application in MRI, the sensing mechanism can also be applied for *ex vivo* detection. Depending on the size of the target biomarker, there are two forms of magnetic NMR assays. For detecting small analytes, such as metabolites, oligonucleotides, and proteins, magnetic relaxation switching (MRSw) effect can be exploited. MRSw relies on the changes in organizational state of magnetic NPs in solution (107). Magnetic NPs switching between dispersed and aggregated states are associated with changes in the spin-spin relaxation time (T_2) (*Figure 5A*). MRSw assays are performed without removing excess unbound magnetic NPs and thereby facilitate the detection of small molecules. On the other hand, larger biological targets (e.g., cellular components, bacteria, and mammalian cells) can be tagged with functional magnetic NPs, while the unbound magnetic NPs are removed. This gain of magnetic signal (change of $1/T_2$) is proportional to the number of bound magnetic NPs and indicates the abundance of relevant biomarkers

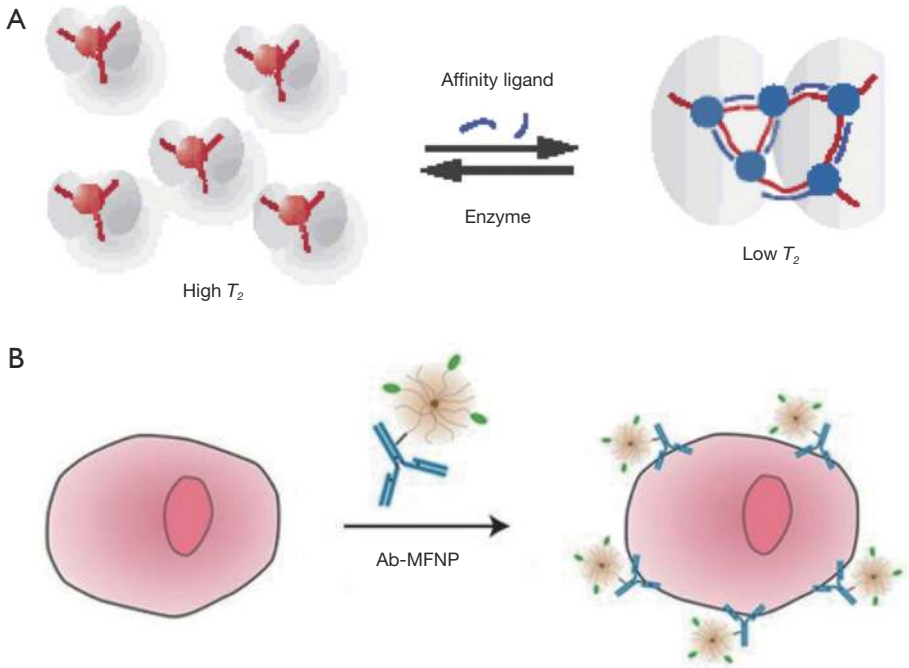

Figure 5 Magnetic assays. (A) Schematic diagram of the MRSw assay. Magnetic NPs switching between dispersed and aggregated states are associated with changes in the spin-spin relaxation time (T_2). The assay is typically applied to detect small biological targets. (B) Magnetic tagging assay. The assay detects the presence of bound magnetic NPs on larger biological entities. Bound magnetic NPs impart a magnetic moment to tagged cells, leading to a decrease in T_2 relaxation time. Unbound magnetic NPs must be removed to ensure detection specificity. Reprinted with permission from (106). Copyright 2002 Nature Publishing Group. Reprinted with permission from (108). Copyright 2010 Nature Publishing Group.

(*Figure 5B*) (7,108). To facilitate these different assay formats, miniaturized NMR detectors have been developed (*Figure 6*). These systems offer distinctive advantages. First, they lower the detection limit by reducing the sample volumes and hence effectively increase the analyte concentrations (109). Second, miniaturized NMR probes (coils) produce much stronger radio-frequency (RF) magnetic fields per unit current, leading to higher signal-to-noise per unit sample volume (101). Third, with smaller RF coils, the requirement for spatial homogeneity of static magnetic fields becomes less stringent, making it possible to use small, portable magnets (34). Through these integrated advances, NMR sensors could be used to detect a wide variety of biological targets, thereby extending its applications for point-of-care biomedical diagnostics.

Discussion

Magnetic NPs and their detection strategies have recently received considerable attention. In combination, these magnetic diagnostic systems offer unique advantages over conventional detection methods. Specifically, because biological samples exhibit negligible magnetic background, magnetic nanomaterials can be used directly for both deep tissue imaging as well as point-of-care diagnostics. Through recent progress in material design and synthesis, new generations of magnetic NPs can be precisely engineered to fulfill new functional needs. For *in vivo* imaging, novel magnetic NPs not only enable strong image contrast of targeted anatomical sites, but can also sense the local molecular environments to catalyze contrast switching. For *ex vivo* diagnostics, magnetic nanomaterials are seamlessly incorporated into miniaturized biosensing platforms, thereby enabling the detection of rare and diverse molecular targets without requiring for extensive sample preparation. Through these synergistic developments, it is likely that magnetic detection will have broad applications in biomedical research as well as clinical translation.

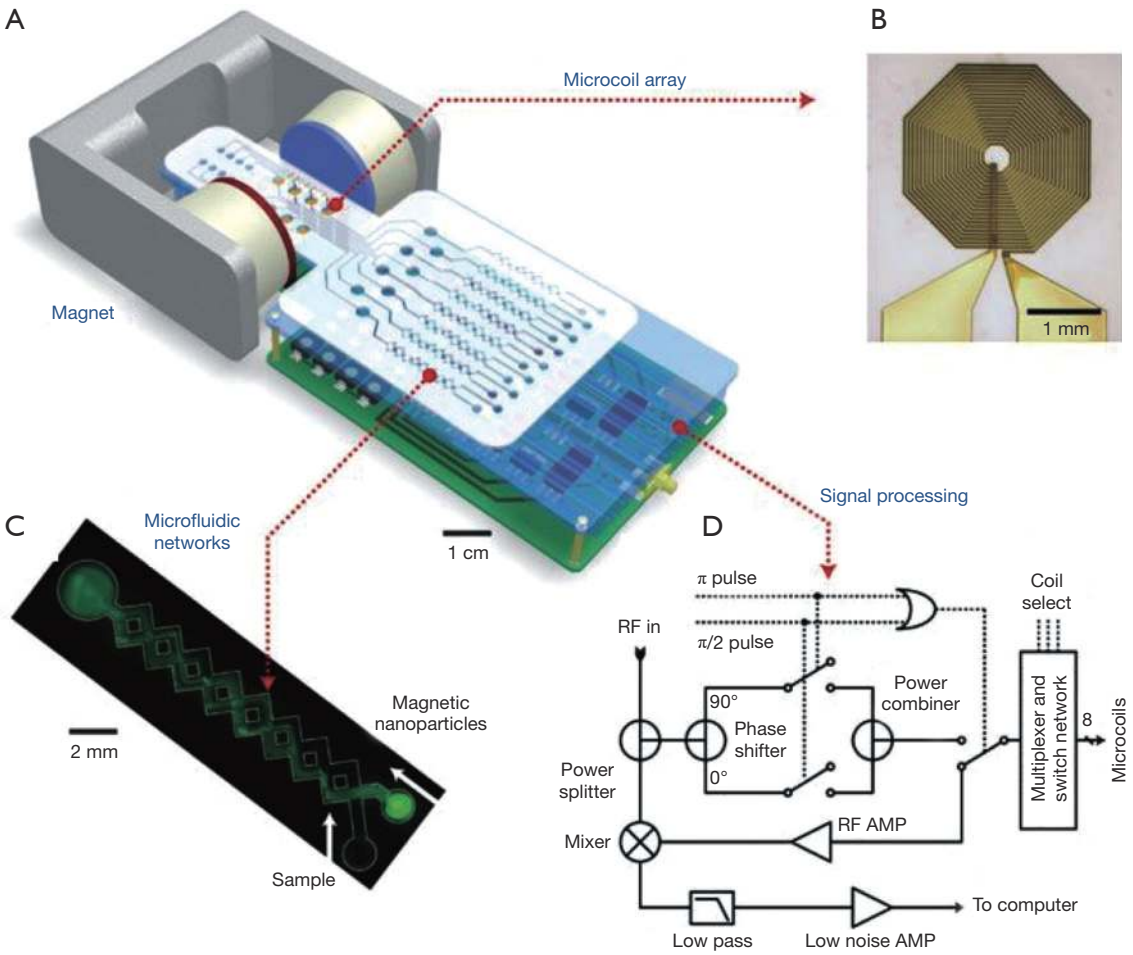

Figure 6 Miniaturized NMR sensors. (A) Schematic diagram of a miniaturized NMR platform. The system consists of (B) an array of microcoils for NMR measurements, (C) microfluidic networks for sample handling and mixing, (D) miniaturized NMR electronics, and a permanent magnet to generate a polarizing magnetic field. Reprinted with permission from (34). Copyright 2008 Nature Publishing Group.

Acknowledgements

This work was supported in part by funding from NUS Research Scholarship, MOE, NMRC, A*STAR IMCB Independent Fellowship and NUS Early Career Research Award.

Footnote

Conflicts of Interest: The authors have no conflicts of interest to declare.

References

1. Wulfkuhle JD, Liotta LA, Petricoin EF. Proteomic applications for the early detection of cancer. Nat Rev Cancer 2003;3:267-75.
2. DeKosky ST, Marek K. Looking backward to move forward: early detection of neurodegenerative disorders. Science 2003;302:830-4.
3. Kalinich M, Haber DA. Cancer detection: Seeking signals in blood. Science 2018;359:866-7.
4. Ludwig JA, Weinstein JN. Biomarkers in cancer staging, prognosis and treatment selection. Nat Rev Cancer 2005;5:845.
5. Shao H, Chung J, Issadore D. Diagnostic technologies for circulating tumour cells and exosomes. Biosci Rep 2015;36:e00292.
6. LaConte L, Nitin N, Bao G. Magnetic nanoparticle probes. Mater Today 2005;8:32-8.
7. Shao H, Min C, Issadore D, Liong M, Yoon TJ, Weissleder

R, Lee H. Magnetic nanoparticles and microNMR for diagnostic applications. Theranostics 2012;2:55-65.
8. Cole AJ, Yang VC, David AE. Cancer theranostics: the rise of targeted magnetic nanoparticles. Trends Biotechnol 2011;29:323-32.
9. Lee H, Shin TH, Cheon J, Weissleder R. Recent Developments in Magnetic Diagnostic Systems. Chem Rev 2015;115:10690-724.
10. Hao R, Xing R, Xu Z, Hou Y, Gao S, Sun S. Synthesis, functionalization, and biomedical applications of multifunctional magnetic nanoparticles. Adv Mater 2010;22:2729-42.
11. Shao H, Yoon TJ, Liong M, Weissleder R, Lee H. Magnetic nanoparticles for biomedical NMR-based diagnostics. Beilstein J Nanotechnol 2010;1:142-54.
12. Yoo D, Lee JH, Shin TH, Cheon J. Theranostic magnetic nanoparticles. Acc Chem Res 2011;44:863-74.
13. Singh A, Sahoo SK. Magnetic nanoparticles: a novel platform for cancer theranostics. Drug Discov Today 2014;19:474-81.
14. Villaraza AJ, Bumb A, Brechbiel MW. Macromolecules, dendrimers, and nanomaterials in magnetic resonance imaging: the interplay between size, function, and pharmacokinetics. Chem Rev 2010;110:2921-59.
15. Wáng YX, Idée JM. A comprehensive literatures update of clinical researches of superparamagnetic resonance iron oxide nanoparticles for magnetic resonance imaging. Quant Imaging Med Surg 2017;7:88-122.
16. Liong M, Shao H, Haun JB, Lee H, Weissleder R. Carboxymethylated polyvinyl alcohol stabilizes doped ferrofluids for biological applications. Adv Mater 2010;22:5168-72.
17. Yoon TJ, Lee H, Shao H, Hilderbrand SA, Weissleder R. Multicore assemblies potentiate magnetic properties of biomagnetic nanoparticles. Adv Mater 2011;23:4793-7.
18. Zhao Z, Zhou Z, Bao J, Wang Z, Hu J, Chi X, Ni K, Wang R, Chen X, Chen Z, Gao J. Octapod iron oxide nanoparticles as high-performance T2 contrast agents for magnetic resonance imaging. Nat Commun 2013;4:2266.
19. Walter A, Billotey C, Garofalo A, Ulhaq-Bouillet C, Lefèvre C, Taleb J, Laurent S, Elst LV, Muller RN, Lartigue L, Gazeau F, Felder-Flesch D, Begin-Colin S. Mastering the shape and composition of dendronized iron oxide nanoparticles to tailor magnetic resonance imaging and hyperthermia. Chem Mater 2014;26:5252-64.
20. Loving GS, Mukherjee S, Caravan P. Redox-activated manganese-based MR contrast agent. J Am Chem Soc 2013;135:4620-3.
21. Chen Y, Yin Q, Ji X, Zhang S, Chen H, Zheng Y, Sun Y, Qu H, Wang Z, Li Y, Wang X, Zhang K, Zhang L, Shi J. Manganese oxide-based multifunctionalized mesoporous silica nanoparticles for pH-responsive MRI, ultrasonography and circumvention of MDR in cancer cells. Biomaterials 2012;33:7126-37.
22. Gao Z, Hou Y, Zeng J, Chen L, Liu C, Yang W, Gao M. Tumor Microenvironment-Triggered Aggregation of Antiphagocytosis 99mTc-Labeled Fe3O4 Nanoprobes for Enhanced Tumor Imaging In Vivo. Adv Mater 2017;29:1701095.
23. Barron LD. Magnetic molecules: Chirality and magnetism shake hands. Nat Mater 2008;7:691-2.
24. Solin SA, Thio T, Hines DR, Heremans JJ. Enhanced room-temperature geometric magnetoresistance in inhomogeneous narrow-gap semiconductors. Science 2000;289:1530-32.
25. Xu Y, Pan HB, He SZ, Li L. A highly sensitive CMOS digital Hall sensor for low magnetic field applications. Sensors (Basel) 2012;12:2162-74.
26. Issadore D, Chung J, Shao H, Liong M, Ghazani AA, Castro CM, Weissleder R, Lee H. Ultrasensitive clinical enumeration of rare cells ex vivo using a micro-hall detector. Sci Transl Med 2012;4:141ra92.
27. Gaster RS, Hall DA, Nielsen CH, Osterfeld SJ, Yu H, Mach KE, Wilson RJ, Murmann B, Liao JC, Gambhir SS, Wang SX. Matrix-insensitive protein assays push the limits of biosensors in medicine. Nat Med 2009;15:1327-32.
28. Gaster RS, Xu L, Han SJ, Wilson RJ, Hall DA, Osterfeld SJ, Yu H, Wang SX. Quantification of protein interactions and solution transport using high-density GMR sensor arrays. Nat Nanotechnol 2011;6:314-20.
29. Shao H, Chung J, Balaj L, Charest A, Bigner DD, Carter BS, Hochberg FH, Breakefield XO, Weissleder R, Lee H. Protein typing of circulating microvesicles allows real-time monitoring of glioblastoma therapy. Nat Med 2012;18:1835-40.
30. Rho J, Chung J, Im H, Liong M, Shao H, Castro CM, Weissleder R, Lee H. Magnetic nanosensor for detection and profiling of erythrocyte-derived microvesicles. ACS Nano 2013;7:11227-33.
31. Shao H, Im H, Castro CM, Breakefield X, Weissleder R, Lee H. New Technologies for Analysis of Extracellular Vesicles. Chem Rev 2018;118:1917-50.
32. Chung HJ, Castro CM, Im H, Lee H, Weissleder R. A magneto-DNA nanoparticle system for rapid detection and phenotyping of bacteria. Nat Nanotechnol 2013;8:369-75.
33. Liong M, Hoang AN, Chung J, Gural N, Ford CB, Min

C, Shah RR, Ahmad R, Fernandez-Suarez M, Fortune SM, Toner M, Lee H, Weissleder R. Magnetic barcode assay for genetic detection of pathogens. Nat Commun 2013;4:1752.
34. Lee H, Sun E, Ham D, Weissleder R. Chip-NMR biosensor for detection and molecular analysis of cells. Nat Med 2008;14:869-74.
35. Le Sage D, Arai K, Glenn DR, DeVience SJ, Pham LM, Rahn-Lee L, Lukin MD, Yacoby A, Komeili A, Walsworth RL. Optical magnetic imaging of living cells. Nature 2013;496:486-9.
36. Bean CP, Livingston JD. Superparamagnetism. J Appl Phys 1959;30:S120-S129.
37. López-López MT, Durán JD, Delgado AV, González-Caballero F. Stability and magnetic characterization of oleate-covered magnetite ferrofluids in different nonpolar carriers. J Colloid Interface Sci 2005;291:144-51.
38. Deng H, Li X, Peng Q, Wang X, Chen J, Li Y. Monodisperse magnetic single-crystal ferrite microspheres. Angew Chem Int Ed Engl 2005;44:2782-5.
39. Yue M, Wang YP, Poudyal N, Rong CB, Liu JP. Preparation of Nd-Fe-B nanoparticles by surfactant-assisted ball milling technique. J Appl Phys 2009;105:07A708.
40. Santra ST, R Theodoropoulou, N, Dobson JH, A, Tan W. Synthesis and characterization of silica-coated iron oxide nanoparticles in microemulsion: the effect of nonionic surfactants. Langmuir 2001;17:2900-6.
41. Woo K, Lee HJ, Ahn JP, Park YS. Sol–gel mediated synthesis of Fe2O3 nanorods. Adv Mater 2003;15:1761-4.
42. Mameli V, Musinu A, Ardu A, Ennas G, Peddis D, Niznansky D, Sangregorio C, Innocenti C, Thanh NT, Cannas C. Studying the effect of Zn-substitution on the magnetic and hyperthermic properties of cobalt ferrite nanoparticles. Nanoscale 2016;8:10124-37.
43. LaMer VK, Dinegar RH. Theory, production and mechanism of formation of monodispersed hydrosols. J Am Chem Soc 1950;72:4847-54.
44. Yoon TJ, Shao H, Weissleder R, Lee H. Oxidation Kinetics and Magnetic Properties of Elemental Iron Nanoparticles. Part Part Syst Charact 2013;30:667-71.
45. Farrell D, Majetich SA, Wilcoxon JP. Preparation and characterization of monodisperse Fe nanoparticles. J Phys Chem B 2003;107:11022-30.
46. Dumestre F, Chaudret B, Amiens C, Renaud P, Fejes P. Superlattices of iron nanocubes synthesized from Fe[N(SiMe3)2]2. Science 2004;303:821-3.
47. Chen M, Liu JP, Sun S. One-step synthesis of FePt nanoparticles with tunable size. J Am Chem Soc 2004;126:8394-5.
48. Wang C, Peng S, Lacroix LM, Sun S. Synthesis of high magnetic moment CoFe nanoparticles via interfacial diffusion in core/shell structured Co/Fe nanoparticles. Nano Res 2009;2:380-5.
49. Cargnello M, Doan-Nguyen VV, Gordon TR, Diaz RE, Stach EA, Gorte RJ, Fornasiero P, Murray CB. Control of metal nanocrystal size reveals metal-support interface role for ceria catalysts. Science 2013;341:771-3.
50. Murray CB, Sun S, Gaschler W, Doyle H, Betley TA, Kagan CR. Colloidal synthesis of nanocrystals and nanocrystal superlattices. IBM J Res Dev 2001;45:47-56.
51. Petit C, Taleb A, Pileni MP. Cobalt nanosized particles organized in a 2D superlattice: synthesis, characterization, and magnetic properties. J Phys Chem B 1999;103:1805-10.
52. Murray CB, Sun S, Doyle H, Betley T. Monodisperse 3d transition-metal (Co, Ni, Fe) nanoparticles and their assembly into nanoparticle superlattices. MRS Bull 2001;26:985-91.
53. Sun S, Murray CB. Synthesis of monodisperse cobalt nanocrystals and their assembly into magnetic superlattices J Appl Phys 1999;85:4325-30.
54. Reddy LH, Arias JL, Nicolas J, Couvreur P. Magnetic nanoparticles: design and characterization, toxicity and biocompatibility, pharmaceutical and biomedical applications. Chem Rev 2012;112:5818-78.
55. Quinto CA, Mohindra P, Tong S, Bao G. Multifunctional superparamagnetic iron oxide nanoparticles for combined chemotherapy and hyperthermia cancer treatment. Nanoscale 2015;7:12728-36.
56. Hou Y, Yu J, Gao S. Solvothermal reduction synthesis and characterization of superparamagnetic magnetite nanoparticles. J Mater Chem 2003;13:1983-7.
57. Lee JH, Huh YM, Jun YW, Seo JW, Jang JT, Song HT, Kim S, Cho EJ, Yoon HG, Suh JS, Cheon J. Artificially engineered magnetic nanoparticles for ultra-sensitive molecular imaging. Nat Med 2007;13:95-9.
58. Zeng H, Rice PM, Wang SX, Sun S. Shape-controlled synthesis and shape-induced texture of MnFe2O4 nanoparticles. J Am Chem Soc 2004;126:11458-9.
59. Wu L, Shen B, Sun S. Synthesis and assembly of barium-doped iron oxide nanoparticles and nanomagnets. Nanoscale 2015;7:16165-9.
60. Redl FX, Black CT, Papaefthymiou GC, Sandstrom RL, Yin M, Zeng H, Murray CB, O'Brien SP. Magnetic, electronic, and structural characterization of nonstoichiometric iron oxides at the nanoscale. J Am Chem Soc 2004;126:14583-99.

61. Ghosh M, Biswas K, Sundaresan A, CN R. MnO and NiO nanoparticles: synthesis and magnetic properties. J Mater Chem 2006;16:106-11.
62. Seo WS, Jo HH, Lee K, Kim B, Oh SJ, Park JT. Size-dependent magnetic properties of colloidal Mn3O4 and MnO nanoparticles. Angew Chem Int Ed Engl 2004;43:1115-7.
63. Wu L, Mendoza-Garcia A, Li Q, Sun S. Organic phase syntheses of magnetic nanoparticles and their applications. Chem Rev 2016;116:10473-512.
64. Zeng H, Sun S. Syntheses, properties, and potential applications of multicomponent magnetic nanoparticles. Adv Funct Mater 2008;18:391-400.
65. Wang C, Xu C, Zeng H, Sun S. Recent progress in syntheses and applications of dumbbell-like nanoparticles. Adv Mater 2009;21:3045-52.
66. Kortan AR, Hull R, Opila RL, Bawendi MG, Steigerwald ML, Carroll PJ, Brus LE. Nucleation and growth of CdSe on ZnS quantum crystallite seeds, and vice versa, in inverse micelle media. J Am Chem Soc 1990;112:1327-32.
67. Lee H, Yoon TJ, Weissleder R. Ultrasensitive detection of bacteria using core-shell nanoparticles and an NMR-filter system. Angew Chem Int Ed Engl 2009;48:5657-60.
68. Yoon TJ, Lee H, Shao H, Weissleder R. Highly magnetic core-shell nanoparticles with a unique magnetization mechanism. Angew Chem Int Ed Engl 2011;50:4663-6.
69. Meffre A, Mehdaoui B, Kelsen V, Fazzini PF, Carrey J, Lachaize S, Respaud M, Chaudret B. A simple chemical route toward monodisperse iron carbide nanoparticles displaying tunable magnetic and unprecedented hyperthermia properties. Nano Lett 2012;12:4722-8.
70. Zeng H, Li J, Wang ZL, Liu JP, Sun S. Bimagnetic core/shell FePt/Fe3O4 nanoparticles. Nano Lett 2004;4:187-90.
71. Shi W, Zeng H, Sahoo Y, Ohulchanskyy TY, Ding Y, Wang ZL, Swihart M, Prasad PN. A general approach to binary and ternary hybrid nanocrystals. Nano Lett 2006;6:875-81.
72. Ge J, Zhang Q, Zhang T, Yin Y. Core-satellite nanocomposite catalysts protected by a porous silica shell: controllable reactivity, high stability, and magnetic recyclability. Angew Chem Int Ed Engl 2008;47:8924-8.
73. Gao J, Liang G, Zhang B, Kuang Y, Zhang X, Xu B. FePt@ CoS2 yolk– shell nanocrystals as a potent agent to kill HeLa cells. J Am Chem Soc 2007;129:1428-33.
74. Jiang J, Gu H, Shao H, Devlin E, Papaefthymiou GC, Ying JY. Bifunctional Fe3O4-Ag heterodimer nanoparticles for two-photon fluorescence imaging and magnetic manipulation. Adv Mater 2008;20:4403-7.
75. Yu H, Chen M, Rice PM, Wang SX, White RL, Sun S. Dumbbell-like bifunctional Au-Fe3O4 nanoparticles. Nano Lett 2005;5:379-82.
76. Wang C, Wei Y, Jiang H, Sun S. Tug-of-war in nanoparticles: competitive growth of Au on Au-Fe3O4 nanoparticles. Nano Lett 2009;9:4544-7.
77. Choi SH, Na HB, Park YI, An K, Kwon SG, Jang Y, MH, Moon J, Son JS, Song IC, Moon WK, Hyeon T. Simple and generalized synthesis of oxide-metal heterostructured nanoparticles and their applications in multimodal biomedical probes. J Am Chem Soc 2008;130:15573-80.
78. Wu B, Tang S, Chen M, Zheng N. Amphiphilic modification and asymmetric silica encapsulation of hydrophobic Au-Fe3O4 dumbbell nanoparticles. Chem Commun (Camb) 2014;50:174-6.
79. Wang YX, Hussain SM, Krestin GP. Superparamagnetic iron oxide contrast agents: physicochemical characteristics and applications in MR imaging. Eur Radiol 2001;11:2319-31.
80. Tong S, Hou S, Zheng Z, Zhou J, Bao G. Coating optimization of superparamagnetic iron oxide nanoparticles for high T2 relaxivity. Nano Lett 2010;10:4607-13.
81. Zhou Z, Huang D, Bao J, Chen Q, Liu G, Chen Z, Chen X, Gao J. A synergistically enhanced T1–T2 dual-modal contrast agent. Adv Mater 2012;24:6223-8.
82. Yang L, Wang Z, Ma L, Li A, Xin J, Wei R, Lin H, Wang R, Chen Z, Gao J. The roles of morphology on the relaxation rates of magnetic nanoparticles. ACS Nano 2018;12:4605-14.
83. Zeng J, Jing L, Hou Y, Jiao M, Qiao R, Jia Q, Liu C, Fang F, Lei H, Gao M. Anchoring group effects of surface ligands on magnetic properties of Fe3 O4 nanoparticles: towards high performance MRI contrast agents. Adv Mater 2014;26:2694-8.
84. Zhou Z, Wang L, Chi X, Bao J, Yang L, Zhao W, Chen Z, Wang X, Chen X, Gao J. Engineered iron-oxide-based nanoparticles as enhanced T1 contrast agents for efficient tumor imaging. ACS Nano 2013;7:3287-96.
85. Na HB, Lee JH, An K, Park YI, Park M, Lee IS, Nam DH, Kim ST, Kim SH, Kim SW, Lim KH, Kim KS, Kim SO, Hyeon T. Development of a T1 contrast agent for magnetic resonance imaging using MnO nanoparticles. Angew Chem Int Ed Engl 2007;46:5397-401.
86. Kim T, Cho EJ, Chae Y, Kim M, Oh A, Jin J, Lee ES, Baik H, Haam S, Suh JS, Huh YM, Lee K. Urchin-shaped manganese oxide nanoparticles as pH-responsive activatable T1 contrast agents for magnetic resonance imaging. Angew Chem Int Ed Engl 2011;50:10589-93.
87. Kim T, Cho EJ, Chae Y, Kim M, Oh A, Jin J, Lee ES, Baik H, Haam S, Suh JS, YM, Lee K. Mesoporous silica-

coated hollow manganese oxide nanoparticles as positive T1 contrast agents for labeling and MRI tracking of adipose-derived mesenchymal stem cells. J Am Chem Soc 2011;133:2955-61.
88. Kim BH, Lee N, Kim H, An K, Park YI, Choi Y, Shin K, Lee Y, Kwon SG, Na HB, Park JG, Ahn TY, Kim YW, Moon WK, Choi SH, Hyeon T. Large-scale synthesis of uniform and extremely small-sized iron oxide nanoparticles for high-resolution T1 magnetic resonance imaging contrast agents. J Am Chem Soc 2011;133:12624-31.
89. De Leon-Rodriguez LM, Lubag AJ, Malloy CR, Martinez GV, Gillies RJ, Sherry AD. Responsive MRI agents for sensing metabolism in vivo. Acc Chem Res 2009;42:948-57.
90. Bennewitz MF, Lobo TL, Nkansah MK, Ulas G, Brudvig GW, Shapiro EM. Biocompatible and pH-sensitive PLGA encapsulated MnO nanocrystals for molecular and cellular MRI. ACS Nano 2011;5:3438-46.
91. Hingorani DV, Bernstein AS, Pagel MD. A review of responsive MRI contrast agents: 2005-2014. Contrast Media Mol Imaging 2015;10:245-65.
92. Osborne EA, Jarrett BR, Tu C, Louie AY. Modulation of T2 relaxation time by light-induced, reversible aggregation of magnetic nanoparticles. J Am Chem Soc 2010;132:5934-5.
93. Gallo J, Kamaly N, Lavdas I, Stevens E, Nguyen QD, Wylezinska-Arridge M, Aboagye EO, Long NJ. CXCR4-targeted and MMP-responsive iron oxide nanoparticles for enhanced magnetic resonance imaging. Angew Chem Int Ed Engl 2014;53:9550-4.
94. Wang L, Huang J, Chen H, Wu H, Xu Y, Li Y, Yi H, Wang YA, Yang L, Mao H. Exerting enhanced permeability and retention effect driven delivery by ultrafine iron oxide nanoparticles with T1-T2 switchable magnetic resonance imaging contrast. ACS Nano 2017;11:4582-92.
95. Baselt DR, Lee GU, Natesan M, Metzger SW, Sheehan PE, Colton RJ. A biosensor based on magnetoresistance technology. Biosens Bioelectron 1998;13:731-9.
96. Ferreira HA, Graham DL, Freitas PP, Cabral JMS. Biodetection using magnetically labeled biomolecules and arrays of spin valve sensors. J Appl Phys 2003;93:7281-6.
97. Miller MM, Prinz GA, Cheng SF, S B. Detection of a micron-sized magnetic sphere using a ring-shaped anisotropic magnetoresistance-based sensor: a model for a magnetoresistance-based biosensor. Appl Phys Lett 2002;81:2211-3.
98. Enpuku K, Minotani T, Gima T, Kuroki Y, Itoh1 Y, Yamashita1 M, Katakura1 Y, Kuhara S. Detection of magnetic nanoparticles with superconducting quantum interference device (SQUID) magnetometer and application to immunoassays. Jpn J Appl Phys 1999;38:L1102.
99. Besse PA, Boero G, Demierre M, Pott V, Popovic R. Detection of a single magnetic microbead using a miniaturized silicon Hall sensor. J Appl Phys 2002;80:4199.
100. Kurlyandskaya G, Levit V. Magnetic Dynabeads detection by sensitive element based on giant magnetoimpedance. Biosens Bioelectron 2005;20:1611-6.
101. Lee H, Yoon TJ, Figueiredo JL, Swirski FK, Weissleder R. Rapid detection and profiling of cancer cells in fine-needle aspirates. Proc Natl Acad Sci U S A 2009;106:12459-64.
102. de Boer BM, Kahlman JA, Jansen TP, Duric H, Veen J. An integrated and sensitive detection platform for magneto-resistive biosensors. Biosens Bioelectron 2007;22:2366-70.
103. Schotter J, Kamp PB, Becker A, Pühler A, Reiss G, Brückl H. Comparison of a prototype magnetoresistive biosensor to standard fluorescent DNA detection. Biosens Bioelectron 2004;19:1149-56.
104. Edelstein RL, Tamanaha CR, Sheehan PE, Miller MM, Baselt DR, Whitman LJ, Colton RJ. The BARC biosensor applied to the detection of biological warfare agents. Biosens Bioelectron 2000;14:805-13.
105. Sun X, Lei C, Guo L, Zhou Y. Separable detecting of Escherichia coli O157H: H7 by a giant magneto-resistance-based bio-sensing system. Sensors and Actuators B: Chemical 2016;234:485-92.
106. Perez JM, Josephson L, O'Loughlin T, Högemann D, Weissleder R. Magnetic relaxation switches capable of sensing molecular interactions. Nat Biotechnol 2002;20:816-20.
107. Min C, Shao H, Liong M, Yoon TJ, Weissleder R, Lee H. Mechanism of magnetic relaxation switching sensing. ACS Nano 2012;6:6821-8.
108. Haun JB, Devaraj NK, Hilderbrand SA, Lee H, Weissleder R. Bioorthogonal chemistry amplifies nanoparticle binding and enhances the sensitivity of cell detection. Nat Nanotechnol 2010;5:660-5.
109. Olson DL, Lacey ME, Sweedler JV. High-resolution microcoil NMR for analysis of mass-limited, nanoliter samples. Anal Chem 1998;70:645-50.

Cite this article as: Chen Y, Ding X, Zhang Y, Natalia A, Sun X, Wang Z, Shao H. Design and synthesis of magnetic nanoparticles for biomedical diagnostics. Quant Imaging Med Surg 2018;8(9):957-970. doi: 10.21037/qims.2018.10.07

